Metavisitor, a suite of Galaxy tools for simple and rapid detection and discovery of viruses in deep sequence data

Guillaume Carissimo[1,2,3], Marius van den Beek[4,5], Juliana Pegoraro[4,5], Kenneth D Vernick[1,2,6] and Christophe Antoniewski[4,5]*

Affiliations:

[1]Institut Pasteur, Unit of Insect Vector Genetics and Genomics, Department of Parasites and Insect Vectors, Paris 75015, FRANCE; [2]CNRS, Unit of Hosts, Vectors and Pathogens (URA3012), Paris 75015, FRANCE; [3]Laboratory of Microbial Immunity, Singapore Immunology Network, A*STAR, 8A Biomedical Grove, Biopolis, Singapore 138648; [4]Sorbonne Universités, Université Pierre et Marie Curie (UPMC), CNRS, Institut de Biologie Paris Seine (IBPS), Developmental Biology Department, F-75005, Paris, France; [5]Sorbonne Universités, Université Pierre et Marie Curie (UPMC), CNRS, Institut de Biologie Paris Seine (IBPS), ARTbio Bioinformatics Analysis Facility, F-75005, Paris, France; [6]Department of Microbiology, University of Minnesota, Minneapolis, MN 55108

*Correspondence: christophe.antoniewski@upmc.fr

Short title: Metavisitor software for viruses discovery in sequence data

Abstract

We present user-friendly and adaptable software to provide biologists, clinical researchers and possibly diagnostic clinicians with the ability to robustly detect and reconstruct viral genomes from complex deep sequence datasets. A set of modular bioinformatic tools and workflows was implemented as the Metavisitor package in the Galaxy framework. Using the graphical Galaxy workflow editor, users with minimal computational skills can use existing Metavisitor workflows or adapt them to suit specific needs by adding or modifying analysis modules. Metavisitor can be used on our Mississippi server, or can be installed on any Galaxy server instance and a pre-configured Metavisitor server image is provided. Metavisitor works with DNA, RNA or small RNA sequencing data over a range of read lengths and can use a combination of *de novo* and guided approaches to assemble genomes from sequencing reads. We show that the software has the potential for quick diagnosis as well as discovery of viruses from a vast array of organisms. Importantly, we provide here executable Metavisitor use cases, which increase the accessibility and transparency of the software, ultimately enabling biologists or clinicians to focus on biological or medical questions.

Introduction

Viruses infect cells and manipulate the host machinery for their replication and transmission. Genomes of viruses show high diversity and can consist of single- or double-stranded RNA or DNA. Many types of viral replication cycles exist which may involve various cellular compartments, various DNA or RNA replication intermediates, and diverse strategies for viral RNA transcription and viral protein translation. Next generation deep-sequencing has become a powerful approach for virologists in their quest to detect and identify viruses in biological samples, even when they are present at low levels. However, none of the existing sequencing methods allows comprehensive detection of all virus classes. For instance, DNA sequencing fails to detect viruses lacking a DNA stage whereas commonly used mRNA sequencing protocols based on poly-A tailed RNA purification fail to detect viruses without poly-A tails.

Plants and invertebrates use RNA interference as an antiviral mechanism (1, 2). Active antiviral RNAi results in significant enrichment of viral interfering small RNAs (viRNAs) relative to endogenous small RNAs (endo-siRNA). The ratio of viRNA reads over endo-siRNA reads depends on several factors such as the ability of a virus to replicate in the host and to evade the host RNAi machinery. Moreover, viRNAs derived from a variety of viruses can be detected in host organisms, regardless if these viruses have positive single strand, negative single strand or double-stranded RNA genomes, or DNA genomes (3). Together, these features make small RNA deep sequencing a potent approach to detect viruses regardless of their genomic specificities, and different bioinformatic tools have been developed for detection or *de novo* assembly of viral genomes.

Accordingly, viRNAs produced by the insect model *Drosophila melanogaster* in response to viral infections were sufficient to reconstruct and improve the genomic consensus sequence of the Nora virus (4) using the Paparazzi perl script (5) which wraps the SSAKE assembler (6). In this study, Paparazzi improved the consensus sequence and the coverage of the Nora virus genome by ~20%, as compared to the previous Nora virus reference genome. SearchSmallRNA, a standalone tool with a graphical interface written in JAVA language, used a similar approach to reconstruct viral genomes (7). Source

codes of both Paparazzi and SearchSmallRNA require specific skills for installation and execution as well as the retrieval of viral reference sequences. Furthermore neither program is currently available for download. Since both programs require known, closely related viral references for proper guidance of genome reconstructions from viRNAs, identification of more distant viral species or discovery of novel or unexpected viruses is precluded.

To circumvent the need for viral reference sequences, Velvet (8) has been used to *de novo* assemble contigs from plant (9), fruit fly and mosquito (10) viRNAs. These contigs have then been aligned to NCBI sequence databases, allowing the identification of partial or complete viral genomes. Several studies improved the strategy by combining two *de novo* assemblers (11–14), or scaffolding the contig pieces that could be blast-aligned to NCBI sequences using an additional translation-guided assembly step (15).

Collectively, the reported work allowed important progress in virus assembly and identification from deep sequencing data. However, the existing computational workflows are poorly accessible to a broad user base of biologists because they require specialist skills for installation, execution and adaptation to specific research. These skills may not be sufficient in some cases where tools are no longer available or documentation is missing.

In this context, we developed Metavisitor as a free and open source set of Galaxy tools and workflows (16, 17) allowing both *de novo* reconstruction of novel viruses and detection of already identified viral species from sequencing datasets. Using the graphical Galaxy workflow editor, Metavisitor workflows can be adapted to suit specific needs, by adding analysis steps or replacing/modifying existing ones. For instance, Metavisitor may help in field surveillance of insect vectors and emerging viral species during epidemics, in viral metagenomic studies or in experimental research or diagnosis for human patients suffering from viral infections or coinfections. In order to improve as much as possible the accessibility and usability of Metavisitor, we detailed a series of use cases that can be directly examined, replayed, tested or adapted using our Galaxy server (http://mississippi.fr). To ensure the sustainability of these executable use cases, a Galaxy server instance provisioned with the Metavisitor tools and workflows is also available as a Docker image. We expect that these tools will provide biologists and

medical practitioners with an easy-to-use and adaptable software for the detection or identification of viruses from NGS datasets.

Methods

Metavisitor consists of a set of Galaxy tools (Figure 1) that can be combined to (i) extract sequencing reads that do not align to the host genomes, known symbionts or parasites; (ii) retrieve up to date nucleotide as well as protein sequences of viral genomes deposited in Genbank (18) and index these sequences for subsequent blast, bowtie, etc. alignments; (iii) perform *de novo* assembly of extracted sequencing reads using Oases or Trinity, align the *de novo* contigs against the viral nucleotide or protein blast databases using blastn or blastx, respectively, and generate reports from blast outputs to help in known viruses diagnosis or in candidate virus discovery; (iv) use CAP3 (optional, see Use Case 3-3), blast and viral scaffolds for selected viruses to generate guided final viral sequence assemblies of blast sequence hits. For clarity, we group analysis steps below in functional tasks (i to iv). However, as shown in the Use Cases section, Metavisitor links these tasks in full workflows that can be executed once to generate complete and adapted analyses.

(i) Prepare data

The purpose of the "Prepare data" task (Figure 1) is to process Illumina sequencing datasets in order to optimize the subsequent *de novo* assembly of viral sequencing reads. Raw sequence files in fastq or fasta format are clipped from library adapters and are converted to a weighted fasta file in which sequences are headed by a character string that contains a unique identifier and the number of times that the sequences were found in the dataset. These steps (which are optional) removes sequence duplicates and drastically reduces the workload of the next steps as well as the coverage variations after de novo assembly (see Use Cases 1-1 to 1-3). Datasets are then depleted from non-viral sequences by sequential alignments to the host genome, to other genomes from known or potential symbionts and parasites, as well as to PhiX174 genome sequences which are commonly used as internal controls in Illumina sequencing and

may contaminate the datasets. The sequence reads that did not match the reference genomes are retained and returned.

(ii) Get reference viral sequences

The "Get reference viral sequences" task is performed using the "Retrieve FASTA from NCBI" tool that sends a query string to the Genbank database (18) and retrieves the corresponding nucleotide or protein sequences. With this tool, a typical query for virus sequences retrieval is "txid10239[Organism] NOT txid131567[Organism] NOT phage", which retrieves viruses sequences (txid10239) while filtering out cellular organisms sequences (txid131567) and phage sequences. This query was submitted to the nucleotide or protein Genbank databases (oct 2015) to retrieve the viral nucleotide and protein databases referred to as "vir1" in the rest of the article. However, users can change the tool settings by entering query strings that fit their specific needs. As downloading large sequence datasets from NCBI may take several hours with this query, we allow users to skip it by directly accessing the nucleotides or protein vir1 datasets on the Mississippi server (http://mississippi.fr) or to download it from figshare (https://dx.doi.org/10.6084/m9.figshare.3179026). For convenience, nucleotide and protein blast indexes are also available in the public library of the Mississippi server (but can also be generated using the "NCBI BLAST+ makeblastdb" Galaxy tool). Bowtie as well as bowtie2 indexes of the vir1 nucleotide sequences have been generated in the Mississippi Galaxy instance using the corresponding "data manager" Galaxy tools.

Finally, users can upload their own viral nucleotide and protein sequences using ftp and transfer them in a Galaxy history (Figure 1).

(iii) Assemble, Blast and Parse

In the task "Assemble, Blast and Parse", RNA sequences returned by the "Prepare data" task are subjected to several rounds of *de novo* assembly by Velvet (8) using the Oases software package (19) and k-mer lengths ranging from 15 to 35 (for small RNA sequences) or from 13 to 69 (for longer RNA sequences). The Oases_optimiser Galaxy tool merges Velvet assemblies obtained at different k-mer lengths into an optimized assembly and returns reconstructed contigs into clusters (loci) of alternate variants. To note, during tests for this batch analysis, we identified a previously unknown bug into

the Oases code, where certain datasets may put the tool in an error state for an unclear reason. Should this happen, shuffling the order of the sequence reads in the dataset fixes the issue. Importantly, as illustrated in Use Case 3-3 (see below), the Oases assembler can be replaced by a different de novo assembler such as Trinity (20) that performs better with longer sequencing reads.

In a next step, *de novo* assembled contigs are aligned to both "virus nucleotides" and "virus proteins" vir1 BLAST databases built from the viral reference sequences (Figure 1) using the blastn or blastx Galaxy tools (21) that search nucleotide or protein databases using nucleotide or translated nucleotide queries, respectively (22). Default parameters for these tools are adjusted in order to report only the 5 best alignments per contig (Maximum hits to show set to 5) and to generate a tabular blast output that includes the 12 standard columns plus a column containing the length of the aligned subject sequences (extended columns, "slen" checked).

Tabular outputs generated by blastn and blastx alignments are next parsed by the "Parse blast output and compile hits" tool to return 4 files. In the "blast analysis, by subjects" output file (Supplementary Figure 1), the subject sequences in the viral nucleotide or protein blast databases that produced significant blast alignments (hits) with Oases contigs are listed, together with those contigs and the blast information associated to the hits (% Identity, alignment Length, start and end coordinates of hits relatively to the subject sequence, percentage of the contig length covered by the hit, E-value and Bit Score of the hit). In addition, for each subject sequence in the list, the length in nucleotide or amino-acid of the subject sequence (Subject Length), the summed coverage of the subject by all contig hits (Total Subject Coverage) as well as the fraction of the subject length that this coverage represents (Relative Subject Coverage), and the best (Best Bit Score) and mean (Mean Bit Score) bit scores produced by contig hits are computed and indicated. A simplified output can be generated without contigs and blast information by using the "compact" option for the reporting mode of the "Parse blast output and compile hits" tool. A second "hits" output file generated by the tool contains the sequences of contig portions that produced significant alignment in the BLAST step (i.e. query hit sequences), flanked by additional contig nucleotides 5' and 3' to the hit (the size of these margins is set to 5 by default and can be modified by the user). Finally,

the tool returns the contigs that produced significant blast hits ("Blast aligned sequences") as well as those that did not ("Blast unaligned sequences").

(iv) Final assembly from blastn or blastx

The last "Final assembly from blastn/x" task (Figure 1) allows to manually choose candidates from user's inspection of the "blast analysis, by subjects" file and to generate further sequence assembly. Using the tool "Pick Fasta sequences" and the appropriate query string, users first retrieve from the file "hits" all blastn or blastx hits that significantly matched a subject sequence. When necessary, these hit sequences can be further assembled in longer contigs using the "cap3 Sequence Assembly" Galaxy tool adapted from CAP3 (23). In some cases (see below), unique viral contigs can already be obtained at this step. In cases where there are still multiple unlinked contigs, the workflow provides the possibility to generate a single composite sequence where these contig sequences (indicated in uppercase characters) are integrated in a matched subject sequence taken as a scaffold (lowercase characters). This is done by (a) retrieving the subject sequence from the NCBI nucleotide databases, generating a blast nucleotide index from this sequence and aligning the contigs to this index with blastn or tblastx tools, and (b) running the "blast_to_scaffold" tools by taking as inputs the contigs, the guide/scaffold sequence and the blastn or blastx output (Figure 1, bottom).

Availability of Metavisitor

All Metavisitor tools are installed in the Galaxy server http://mississippi.snv.jussieu.fr. In addition, all Use Cases described in this article are available on the server through html links in the article. Using these links, readers can directly examine input data, analysis workflows and results histories. Readers can also import the Metavisitor Use Case histories (https://mississippi.snv.jussieu.fr/history/list_published) and Metavisitor Use Case workflows (https://mississippi.snv.jussieu.fr/workflow/list_published) published in Mississippi to re-run the described analyses or adapt them to their studies.

We made all tools and workflows that compose Metavisitor available from the main Galaxy tool shed (https://toolshed.g2.bx.psu.edu/), in the form of a tool suite

(suite_metavisitor_1_2) which thus can be installed and used on any Galaxy server instance. The Metavisitor tools are also accessible in our public repository for code development at https://github.com/ARTbio/tools-artbio/. The Metavisitor workflows generated for the Use Cases described in this article are also available from http://www.myexperiment.org/search?commit=Go&page=1&query=metavisitor. These workflows can be freely modified or complemented with additional analysis steps within the Galaxy environment.

Finally, we provide a Docker image ARTbio/metavisitor:1.2 that allows to deploy a Galaxy server instance with preinstalled Metavisitor tools and workflows in local infrastructures.

Results / Uses Cases

In this section, we present use cases to demonstrate the use of various Metavisitor workflows adapted to specific situations and dataset formats. For each use case, we briefly present the purpose of the original study from which the datasets originate, and we propose html links to input data, workflows as well as to histories generated with these workflows and input data. Using this process, we intend to provide transparent and executable analyses: readers can examine the use cases in every detail using the Galaxy web interface; they can also import the input data, histories and workflows in their own Galaxy Mississippi account and re-execute the analyses as we did; finally they can experiment Metavisitor workflows with their own datasets and parameters.

1. Detection of known viruses

Use Cases 1-1, 1-2 and 1-3

Using small RNA sequencing libraries SRP013822 (EBI ENA) and the Paparazzi software (5) we were previously able to propose a novel reference genome (NCBI JX220408) for the Nora virus strain infecting Drosophila melanogaster stocks in laboratories (4). This so-called rNora genome differed by 3.2% nucleotides from the Nora virus reference NC_007919.3 and improved the alignment rate of viral siRNAs by ~121% . Thus, we first tested Metavisitor on the small RNA sequencing datasets SRP013822.

Three Metavisitor workflows were run on the merged SRP013822 small RNA sequence reads and the NC_007919.3 genome as a guide for final reconstruction (in Galaxy history "Input data for Use Cases 1-1, 1-2, 1-3 and 1-4"). The first Workflow for Use Case 1-1 used raw reads collapsed to unique sequences (see methods section) to reconstruct a Nora virus genome referred to as Nora_MV (dataset 35) in the History for Use Case 1-1. In a second Workflow for Use Case 1-2, we did not collapse the SRP013822 reads to unique sequences (see materials and method), which allowed the reconstruction of a Nora raw reads genome (dataset 33) in the History for Use Case 1-2. In a third Workflow for Use Case 1-3, the abundances of SRP013822 sequence reads were normalized using the Galaxy tool "Normalize by median" (24), which allowed the reconstruction of a Nora Median-Norm-reads genome (dataset 37) in the History for Use Case 1-3.

All three reconstructed genomes as well as the Paparazzi-reconstructed JX220408 genome had a high sequence similarity (>96.6% nucleotide identity) with the NC_007919.3 guide genome (see Supplementary File 1). The final *de novo* (capital letters) assemblies of both the Nora_raw_reads and Nora_Median-Norm-reads genomes entirely covered the JX220408 and NC_007919.3 genomes (both 12333 nt), whereas the *de novo* assembled part of the Nora_MV genome was marginally shorter (12298nt, the 31 first 5' nucleotides are in lowercase to indicate that they were not *de novo* assembled but instead recovered from the guide genome). To evaluate the quality of assemblies, we use the "Workflow for remapping in Use Cases 1-1,2,3" (from the history Input data for Use Cases 1-1, 1-2, 1-3 and 1-4) for remapping of the SRP013822 raw reads to the 3 reconstituted Nora virus genomes as well as to the JX220408 guide genome. As can be seen in "History for remapping in Use Cases 1-1,2,3" and Fig. 2, SRP013822 reads matched the genomes with almost identical profiles and had characteristic size distributions of viral siRNAs with a major peak at 21 nucleotides. Importantly, the numbers of reads re-matched to the Nora virus genomes were 1,578,704 (Nora_MV) > 1,578,135 (Paparazzi - JX220408) > 1,566,909 (Nora_raw_reads) > 1,558,000 (Nora_Median-Norm-reads) > 872,128 (NC_007919.3 reference genome guide).

Thus, Metavisitor reconstructed a Nora virus genome Nora_MV whose sequence maximizes the number of vsiRNA read alignments which suggests it is the most accurate

genome for the Nora virus present in the datasets. Of note, the Nora_MV genome differs from the JX220408 rNora genome generated by Paparazzi by only two mismatches at positions 367 and 10707, and four 2nt-deletions at positions 223, 365, 9059 and 12217 (see Supplementary File 1). These variations did not change the amino acid sequence of the 4 ORFs of the Nora virus. We conclude that Metavisitor performs slightly better than Paparazzi for a known virus, using *de novo* assembly of small RNA reads followed by blast-guided assembly. We did not observe any benefits of using raw reads (Metavisitor Use Case 1-2) or normalized-by-median reads (Metavisitor Use Case 1-3) for the Oases assembly, but rather a decrease in the accuracy of the reconstructed genome as measured by the number of reads re-mapped to the final genomes (Figure 2).

Use Case 1-4

In order to show the ability of Metavisitor in detecting multiple known viruses in small RNA sequencing datasets, we derived a simplified workflow from the "Workflow for Use Case 1-1", where blastn alignments of Oases contigs are simply parsed using the "Parse blast output and compile hits" tool without any filtering. Using this Workflow for Use Case 1-4 with the SRP013822 sequence datasets as input returned a list of parsed blastn alignments in the "History for Use Case 1-4" which contains, as expected, the Nora virus. In addition, Oases contigs were found to align with high significance (Mean BitScore > 500) to the Drosophila A virus and to the Drosophila C virus (Dataset 18 and Table 1), strongly suggesting that the fly stocks analyzed in our previous work were also subject to persistent infection by these viruses (4).

2. Discovery of novel viruses

Use Case 2-1

We recently discovered two novel viruses infecting a laboratory colony of *Anopheles coluzzii* mosquitoes (Carissimo et al., PLoS ONE, in press). Using small RNA datasets from these mosquitoes (study accession number ERP012577, history "Input data for Use Cases 2-1 and 2-2"), and the Workflow for Use Case 2-1, we were able to assemble a number a Oases contigs that showed significant blastx hits with *Dicistroviridae* proteins, including *Drosophila* C virus (DCV) and Cricket paralysis virus (CrPV) proteins (see the dataset 26 produced by the "Parse blast output and compile hits" tools in the History for

Use Case 2-1. The viral family of *Dicistroviridae* was named from the dicistronic organisation of their genome. A 5' open reading frame codes for a non-structural polyprotein and a second non-overlapping 3' open reading frame codes for the structural polyprotein of the viral particle.

In order to construct a potential new *A. coluzzii* dicistrovirus genome, we thus collected blastx hits showing significant alignment with both *Drosophila* C virus and *Cricket* paralysis viral polyproteins (dataset 32, Dicistroviridae Hits), and we further assembled these hits using CAP3, which produced 4 contigs of 1952, 341, 4688 and 320 nt, respectively. We then aligned these 4 contigs to the DCV genome NC_001834.1 with tblastx and used the "blast_to_scaffold" tool to produce a final assembly (dataset 42: "New AnCV sequences in DCV scaffold"). Re-mapping of the ERP012577 small RNA reads using the Workflow for remapping in Use Cases 1-1,2,3 adapted to ERP012577 at runtime showed that they mostly align to *de novo* assembled regions (uppercase nucleotides) of this chimeric genome and have a typical size distribution of viral derived siRNA (see dataset 64), suggesting that the NC_001834.1 DCV sequences of the scaffold (lowercase nucleotides) are loosely related to the actual sequence of the novel *Anopheles coluzzii* dicistrovirus. Nevertheless, the composite assembly already allows designing primers in the *de novo* assembled regions to PCR amplify and sequence the regions of the viral genome that could not be *de novo* assembled.

Use Case 2-2

We next used RNAseq libraries from the same *Anopheles coluzzii* colony available in the history Input data for Use Cases 2-1 and 2-2 (dataset 19, deposited in EBI-SRA under accession number ERS977505) to demonstrate the use of a Metavisitor workflow with long RNA sequencing read datasets. Thus, to generate the Galaxy History for Use Case 2-2 with the Workflow for Use Case 2-2, 100nt reads were aligned without any clipping to the *Anopheles gambiae* genome using bowtie2, and unmatched read were subjected to Oases assembly (kmer range, 25 to 69). Oases contigs were then filtered for a size > 5000 nt and aligned to the protein viral reference using blastx. Parsing of blastx alignments with the "blast analysis, by subjects" tool repeatedly pointed to a 8919nt long Oases contig that matched to structural and non-structural polyproteins of DCV and CrPV (dataset 24 in history for Use Case 2-2). This 8919nt contig (dataset 29 in History

for Use Case 2-2) completely includes the contigs generated with the small RNA datasets and shows a dicistronic organization which is typical of Dicistroviridae and is referred to as a novel *Anopheles* C Virus (AnCV, Carissimo et al., PLoS ONE, in press). The sequence of this *Anopheles* C Virus is deposited to the NCBI nucleotide database under accession number KU169878. As expected, the ERP012577 small RNA reads realigned to this genome (using the Workflow for remapping in Use Cases 2-1,2) now show a typical alignment profile all along the AnCV genome sequence with a size distribution peaking at the 21nt length of viral derived siRNAs and no gap (dataset 84: Size distribution and Readmaps in Galaxy history Metavisitor Use Case 2-2).

Taken together, the Metavisitor Use Cases 2-1 and 2-2 illustrate that when short read datasets do not provide enough sequencing information, a simple, adapted Metavisitor workflow is able to exploit long reads of RNA sequencing datasets, if available, to assemble a complete viral genome.

3. Virus detection in human RNAseq libraries

Having illustrated that Metavisitor is able to generate robust genome assemblies from known and novel viruses in *Drosophila* and *Anopheles* sequencing datasets, we tested whether it can be used as a diagnostic workflow to detect viruses in RNA sequencing datasets of human patients from three different studies (25–27).

Use Case 3-1

Innate lymphoid cells (ILCs) play a central role in response to viral infection by secreting cytokines crucial for immune regulation, tissue homeostasis, and repair. Therefore, the pathogenic effect of HIV on these cells was recently analyzed in infected or uninfected patients using various approaches, including transcriptome profiling (26). ILCs are unlikely to be infected *in vivo* by HIV as they lack expression of the CD4 co-receptor of HIV and they are refractory *in vitro* to HIV infection. However, we reasoned that ILCs samples could still be contaminated by infected cells. This might allow Metavisitor to detect and assemble HIV genomes from patient's ILC sequencing data (EBI SRP068722). As these datasets contains short 32 nt reads which in addition had to be 3' trimmed to 27 nt to retain acceptable sequence quality, we designed a Workflow for Use Case 3-1 that is similar to the workflows used in cases 1-1 and 2-1 for small RNA sequencing data.

In that workflow however, sequencing datasets are depleted from reads aligning to the human genome (hg19) and viral reads are selected by alignment to the NCBI viral sequences using our sRbowtie tool. These reads are further submitted to Oases assembly (kmers 11 to 27), the resulting contigs are aligned to the Nucleotide Viral Blast Database using blastn. Alignments are parsed using the "Parse blast output and compile hits" tool, removing alignments to NCBI sequences related to patents to simplify the report ("Patent" term in the filter option of the "Parse blast output and compile hits" tool). Finally, a report is generated by concatenating the reports produced by this tool for each patient.

Using the Galaxy tool "Extract reads in FASTQ/A format from NCBI SRA", we imported 40 sequence datasets from the EBI SRP068722 archive in the history "Input data for Use Case 3-1" and we merged the ICL datasets belonging to the same patients (datasets 43 to 59). We then generated a dataset collection of these patient sequence data (Patient collection) and executed the Workflow for Use Case 3-1 to perform all-in-one batch analysis of this collection in the History for Use Case 3-1 (summarized in Table 2). In this history analysis, we were able to detect HIV RNAs in samples from 3 out of 4 infected patients whereas all samples from control uninfected patients remained negative for HIV. This Metavisitor workflow was able to accurately detect HIV RNA, even in samples where the number of sequence reads was expected to be low, as mentioned above.

Use Case 3-2

Yozwiak *et al.* searched the presence of viruses in RNA Illumina sequencing data from serums of children suffering from fevers of unknown origins (25). In this study, paired-end sequencing datasets were depleted from reads aligning to the human genome and the human transcriptome using BLAT and BLASTn, respectively, and the remaining reads were aligned to the NCBI nucleotide database using BLASTn. A virus was considered identified when 10 reads or more aligned to a viral genome which was not tagged as a known lab contaminant.

For a significant number of Patient IDs reported in table 1 of the article (25), we were not able to find the corresponding sequencing files in the deposited EBI SRP011425 archive. In addition, we did not find the same read counts for these datasets as those indicated by the authors. With these limitations in mind, we used the Galaxy tool

"Extract reads in FASTQ/A format from NCBI SRA" to download in the Galaxy history "Input Data for Use Case 3-2" 86 sequencing datasets that could be further concatenated and assigned to 36 patients in Yozwiak *et al* (25) (dataset collection 191). It is noteworthy that sequence reads in SRP011425 datasets are 97 nt long. Thus, the "Workflow for Use Case 3-2" that we built to perform all-in-one batch analysis is adapted from the Workflow for Use Case 3-1 with the following modifications: (i) sequences reads are depleted from human sequences and viral reads are selected by alignment to the NCBI viral sequences using the Galaxy bowtie2 tool instead of our sRbowtie tool; (ii) viral reads are submitted to Oases assembly using kmer values ranging from 13 to 69; (iii) the SAM file with reads alignments to the vir1 bowtie2 index is parsed using the "join" and "sort" Galaxy tools in order to detect putative false negative datasets with viral reads that fails to produce significant Oases viral contigs.

We executed the Workflow for Use Case 3-2 on the datasets from the history "Input Data for Use Case 3-2" to produce the History for Use Case 3-2. The information generated in this history is summarized in Table 3 (see also the dataset 484 "Virus identification by patient") and shows that under these settings, Metavisitor detected the same viruses as those reported by Yozwiak *et al.* in 17 patients. Although viral reads were detected in 16 other patients, they were not covering sufficient portions of viral genomes to produce significant viral assemblies. Finally, in the three remaining patients (patients 363, 330 and 345 in Table 3 and corresponding Galaxy datasets datasets 424, 384 and 368), we detected viruses (Dengue virus 2, Stealth virus 1 and Dengue virus 4, respectively) other than those identified by Yozwiak *et al*. As mentioned above, these discrepancies are most likely due to misannotation of deposited datasets, which precludes further detailed comparisons.

Use case 3-3

Matranga *et al.* recently improved library preparation methods for deep sequencing of Lassa and Ebola viral RNAs in clinical and biological samples (27). Accordingly, they were able to generate sequence datasets of 150 nt reads providing high coverage of the viral genomes. We used these datasets, relevant in the context of Lassa and Ebola outbreak and epidemic response, to demonstrate the versatility of Metavisitor as well as its ability to generate high throughput reconstruction of viral genomes.

In order to take into account the longer reads and higher viral sequencing depths in the available datasets (27), we adapted a Metavisitor workflow for Use Case 3-3 as follows: (i) The sequencing reads are directly aligned to the viral NCBI sequences without prior depletion by alignment to the human or rodent hosts; (ii) the Trinity *de novo* assembler (20) that performs well with longer reads is used instead of Oases; (iii) reconstruction of Lassa and Ebola genomes from the sequences of the blast hits with the nucleotide viral blast database is directly performed with our blast to scaffold tool without CAP3 assembly since the Trinity contigs are already covering a significant part of the viral genomes; (iv) the reports generated by our "Parse blast output and compile hits" tool as well as the reconstructed genome generated for each sample are concatenated in single datasets for easier browsing and subsequent phylogenetic or variant analyses; (v) finally, for adaptability to any type of virus, two input variables are specified by the user at the workflow runtime: the name of the virus to be searched for in the analysis, and the identifier of the sequence to be used as guide in genome reconstruction steps.

We imported 63 sequence datasets available in the EBI SRA PRJNA254017 and PRJNA257197 archives (27) in the history "Input Data for Use Case 3-3", and grouped these datasets in Lassa virus (55 fastq files) and Ebola virus (8 fastq files) dataset collections (see Table 4 for the complete description of the analyzed samples). To generate the History for Use Case 3-3 Lassa L, we then executed the workflow for Use Case 3-3, taking the Lassa virus dataset collection as input sequences, "Lassa" as a filter term for the "Parse blast output and compile hits" tool and the NCBI sequence NC_004297.1 as a guide for reconstruction of the Lassa virus segment L. We also generated the History for Use Case 3-3 Ebola with the same workflow, taking the Ebola virus dataset collection as input sequences, "Ebola" as a filter term for the "Parse blast output and compile hits" tool and the NCBI sequence NC_002549.1 as a guide for reconstruction of the Ebola virus genome.

The results of both analyses are summarized in Table 4. Metavisitor was able to detect Ebola virus in all corresponding sequence datasets as well as Lassa virus in 53 out the 55 sequence datasets generated from Lassa virus samples. Importantly, Matranga *et al* also did not report reconstructed Lassa genomic segments from the two datasets that we found to be Lassa virus negative, likely due to high read duplication levels in the

corresponding libraries (27). The reconstructed Lassa virus L segments are compiled in the dataset 679 of History for Use Case 3-3 Lassa L whereas reconstructed Ebola virus genomes are compiled in the dataset 115 of History for Use Case 3-3 Ebola. In these sequences, *de novo* assembled segments in uppercases are integrated in the reference guide sequence (lowercase) used for the reconstruction. To note, for viruses with segmented genomes the workflow for Use Case 3-3 has to be used separately with corresponding guide sequences for the appropriate segment to be reconstructed. As an example, we used this workflow with the input variables "Lassa" (filter term for the "Parse blast output and compile hits" tool) and "NC_004296.1" (Lassa S segment used for guiding the reconstruction) to generate the History for Use Case 3-3 Lassa S.

At this stage, users can use the genomic fasta sequences for further analyses. For instance, multiple sequence alignments) can be directly performed for phylogenetics or variant analyses, or reads in the original datasets can be realigned to the viral genomes as in Use Cases 1 and 2 to visualize their coverages.

Discussion

In order to address accessibility, reproducibility and transparency issues in bioinformatics analyses for the detection and reconstruction of viruses, we developed Metavisitor, an open-source suite of tools and workflows executable in Galaxy. Galaxy provides a framework supported by a growing community, and allows executing computational tools and workflows through a user-friendly web interface without need for advanced skills in bioinformatics. Thus, on the one hand, Metavisitor may be useful to many researchers, from seasoned bioinformaticians to medical virologists trying to identify the source of an unknown illness. On the other hand, the advanced Galaxy functionalities ensure the highest levels of computational analyses, through rigorous recording of the produced data and metadata and of the used parameters as well as the ability to share, publish and reproduce these analyses, as illustrated by this work. Another major benefit from their integration in Galaxy is that, as any Galaxy workflow, the Metavisitor workflows may easily be adapted, modified or extended with tools from the active Galaxy developer community.

Through use cases, we have shown that the current set of Metavisitor tools can generate workflows adapted to diverse situations: (a) Short or longer reads from small RNAseq, RNAseq or DNAseq can be used as input data, in a fastq or fasta format, with or without clipping adapter sequences. (b) Sequence information in these input data can be used as is, or compressed using our reads-to-sequences procedure or normalization by median (24). This compression greatly reduces the workload and may improve the quality of the *de novo* assembly step (see Use Cases 1-1 to 1-3). (c) We used three alignment tools in this work based on Bowtie or Bowtie2, including our sRbowtie tool adapted to short RNA reads. Indeed any alignment software producing BAM/SAM outputs may be used in future Metavisitor workflows, provided that they are wrapped for their integration in the Galaxy framework. (d) We have shown the benefit of subtracting non-viral reads before *de novo* assembly by their alignment to host, parasite or symbiont genomes. Nevertheless, Use Case 3-3 illustrates that this step is optional when experimental procedures generate sequence datasets highly enriched in viral sequences. (e) We adapted efficient workflows for two *de novo* assembler programs (Oases and Trinity). It is noteworthy that both of these assemblers could be used in parallel in a single Metavisitor workflow to produce more contigs, which are subsequently filtered by blastn/x alignments to known viral sequences. Any other *de novo* assembly software can be adapted to be used as Metavisitor assembly tool. (f) The viral genome reconstruction can also be adapted. We found that when the number of blast hits to the guide sequences is high, indicative of a high coverage, then the CAP3 assembly of the corresponding hit sequences may be omitted. For instance, our tool "blast_to_scaffold" was sufficient to generate full Lassa and Ebola genome reconstructions in Use Case 3-3. (g) Finally, central to Metavisitor are the viral nucleotide and protein references used in the workflows to identify viral contigs or viral reads. We retrieved the vir1 references from the NCBI using the "Retrieve FASTA from NCBI" Galaxy tool with an explicit query string. We will re-run this tool on a regular basis with the same query string to update the vir1 references with sequences newly deposited to the NCBI databases. However, users are free to adapt Metavisitor workflows to their own viral references either by running the "Retrieve FASTA from NCBI" tool using query strings of there choice or by uploading their own fasta sequences. This is possible since alignment tools in the Metavisitor tool

suite, including sRbowtie, Bowtie, Bowtie2 and Blast, can work with indexes generated on the fly from fasta datasets present in Galaxy users' histories.

A modular and scalable software for biologists and clinicians

Metavisitor tools are modules that can be combined by biologists and clinicians to build analyses workflows adapted to their needs: from detection or reconstruction of known viruses in *Drosophila* small RNA-seq datasets to novel virus discovery in *Anopheles* (Carissimo et al, PLoS ONE, in press) to diagnosis and reconstruction of viruses of patients from RNA-seq datasets. Importantly we showed that Metavisitor is able to detect co-infections by multiple viruses (see Use Case 1-4 for an example).

Viral genome sequences reconstructed by Metavisitor can be used for any subsequent analysis, including phylogenetic or genetic drift analyses in contexts of epidemics or viruses surveillance in field insect vectors, animal or human populations, and systematic identification of viruses for evaluation of their morbidity. The use of Galaxy dataset collections allows to adapt Metavisitor to high throughput analyses. For instance, in Use Cases 3-1 to 3-3 we were able to analyze in batch dozens of patient data from multiplexed sequencing experiments, with consistent tracking of individual samples, from fastq datasets to individual viral genome reconstruction. Thus we are confident that Metavisitor is scalable to large epidemiological studies or to clinical diagnosis in hospital environments. One possible immediate exploitation of this scalability would be to reconstruct sequences of the Zika virus strains from infected patients and identify possible co-infections that could explain and correlate with clinical symptoms.

Future directions

The central idea in Metavisitor is to detect *de novo* contigs of viral sequence reads through blast alignments. Indeed, the ability to form *de novo* viral contigs that align to the large viral sequence database extracted from Genbank NCBI (vir1) provides very strong evidence of the presence of a virus while ensuring a low rate of false positives. However, this current vir1 reference database is redundant and contains sequences whose annotations are misleading or not meaningful (for instance, chimeric sequences between host and viral genomes or patent sequences). We will work at removing redundant or mis-annotated sequences from vir1. This curated vir1 reference will

improve the speed of the alignment steps, reduce the size of the reports generated by Metavisitor while including phylogenetic informations on detected viruses. In the meantime, the versatility of Metavisitor allows users to work with their own viral sequence references.

We are aware that low viral loads in sequenced samples and/or viral read alignments to scattered short regions of viral genomes may result in failure to assemble viral contigs and thus in putative false negatives. We have shown how to keep track of these false negatives in the Workflow for Use Case 3-2 by parsing the SAM alignments to the vir1 index in order to annotate and to count viral reads before the contig assembly steps (Table 3). This tracking of putative false negatives will also be simplified with a curated vir1 reference.

We finally wish to stress that Metavisitor has the potential for integrating detection or diagnosis of non-viral, microbial components in biological samples. Eukaryotic parasites or symbionts and bacteria are mostly detectable in sequencing datasets from their abundant ribosomal RNAs whose sequences are strongly conserved in the main kingdoms. This raises specific issues for their accurate identification and their taxonomic resolution which are not currently addressed by Metavisitor. However, many tools and databases (28) addressing these metagenomics challenges can be adapted, when not already, to the Galaxy framework. For instance, Qiime (29) and the SILVA database of ribosomal RNAs (30) can be used within Galaxy and could thus be integrated in future Metavisitor workflows.

Funding

This work received financial support to CA from the Agence Nationale de la Recherche grant ANR-13-BSV2-0007 « Plastisipi » and from the Institut Universitaire d'Ingéniérie en Santé IUIS grant "ARTiMED" and to KDV from the European Research Council (http://erc.europa.eu/funding-and-grants), Support for frontier research, Advanced Grant #323173 AnoPath; European Commission (http://ec.europa.eu/research/fp7), FP7 Infrastructures #228421 Infravec; and French Laboratoire d'Excellence (http://www.enseignementsup-recherche.gouv.fr/cid55551/investissements-d-avenir-

projets-laboratoires-d-excellence-par-region-et-domaine.html), "Integrative Biology of Emerging Infectious Diseases" #ANR-10-LABX-62-IBEID.

The funders had no role in study design, data collection and analysis, decision to publish, or preparation of the manuscript.

Acknowledgements

We thank the Galaxy community for their support and Eugeni Belda and Emmanuel Bischoff for helpful discussions. GC, MvdB and CA conceived the project. CA and MvdB developed and implemented tools in the Galaxy framework. GC, MvdB, JP and CA performed bioinformatics analysis. GC, MvdB, KV and CA wrote the manuscript. CA and KV provided funding. All authors read and approved the final manuscript.

References

1. Kingsolver,M.B., Huang,Z. and Hardy,R.W. (2013) Insect antiviral innate immunity: pathways, effectors, and connections. *J. Mol. Biol.*, **425**, 4921–4936.

2. Ding,S.-W. and Voinnet,O. (2007) Antiviral immunity directed by small RNAs. *Cell*, **130**, 413–426.

3. Koonin,E.V., Dolja,V.V. and Krupovic,M. (2015) Origins and evolution of viruses of eukaryotes: The ultimate modularity. *Virology*, **479-480C**, 2–25.

4. van Mierlo,J.T., Bronkhorst,A.W., Overheul,G.J., Sadanandan,S.A., Ekström,J.-O., Heestermans,M., Hultmark,D., Antoniewski,C. and van Rij,R.P. (2012) Convergent evolution of argonaute-2 slicer antagonism in two distinct insect RNA viruses. *PLoS Pathog.*, **8**, e1002872.

5. Vodovar,N., Goic,B., Blanc,H. and Saleh,M.-C. (2011) In silico reconstruction of viral genomes from small RNAs improves virus-derived small interfering RNA profiling. *J. Virol.*, **85**, 11016–11021.

6. Warren,R.L., Sutton,G.G., Jones,S.J.M. and Holt,R.A. (2007) Assembling millions of short DNA sequences using SSAKE. *Bioinformatics*, **23**, 500–501.

7. de Andrade,R.R.S. and Vaslin,M.F.S. (2014) SearchSmallRNA: a graphical interface tool for the assemblage of viral genomes using small RNA libraries data. *Virol. J.*, **11**, 45.

8. Zerbino,D.R. and Birney,E. (2008) Velvet: algorithms for de novo short read assembly using de Bruijn graphs. *Genome Res.*, **18**, 821–829.

9. Kreuze,J.F., Perez,A., Untiveros,M., Quispe,D., Fuentes,S., Barker,I. and Simon,R. (2009)

Complete viral genome sequence and discovery of novel viruses by deep sequencing of small RNAs: a generic method for diagnosis, discovery and sequencing of viruses. *Virology*, **388**, 1–7.

10. Wu,Q., Luo,Y., Lu,R., Lau,N., Lai,E.C., Li,W.-X. and Ding,S.-W. (2010) Virus discovery by deep sequencing and assembly of virus-derived small silencing RNAs. *Proc. Natl. Acad. Sci. U. S. A.*, **107**, 1606–1611.

11. Seguin,J., Rajeswaran,R., Malpica-López,N., Martin,R.R., Kasschau,K., Dolja,V.V., Otten,P., Farinelli,L. and Pooggin,M.M. (2014) De novo reconstruction of consensus master genomes of plant RNA and DNA viruses from siRNAs. *PLoS One*, **9**, e88513.

12. Ho,T. and Tzanetakis,I.E. (2014) Development of a virus detection and discovery pipeline using next generation sequencing. *Virology*, **471-473**, 54–60.

13. Aguiar,E.R.G.R., Olmo,R.P., Paro,S., Ferreira,F.V., de Faria,I.J. da S., Todjro,Y.M.H., Lobo,F.P., Kroon,E.G., Meignin,C., Gatherer,D., *et al.* (2015) Sequence-independent characterization of viruses based on the pattern of viral small RNAs produced by the host. *Nucleic Acids Res.*, 10.1093/nar/gkv587.

14. Webster,C.L., Waldron,F.M., Robertson,S., Crowson,D., Ferrari,G., Quintana,J.F., Brouqui,J.-M., Bayne,E.H., Longdon,B., Buck,A.H., *et al.* (2015) The Discovery, Distribution, and Evolution of Viruses Associated with Drosophila melanogaster. *PLoS Biol.*, **13**, e1002210.

15. Surget-Groba,Y. and Montoya-Burgos,J.I. (2010) Optimization of de novo transcriptome assembly from next-generation sequencing data. *Genome Res.*, **20**, 1432–1440.

16. Goecks,J., Nekrutenko,A., Taylor,J. and Galaxy Team (2010) Galaxy: a comprehensive approach for supporting accessible, reproducible, and transparent computational research in the life sciences. *Genome Biol.*, **11**, R86.

17. Blankenberg,D., Von Kuster,G., Coraor,N., Ananda,G., Lazarus,R., Mangan,M., Nekrutenko,A. and Taylor,J. (2010) Galaxy: a web-based genome analysis tool for experimentalists. *Curr. Protoc. Mol. Biol.*, **Chapter 19**, Unit 19.10.1–21.

18. Benson,D.A., Cavanaugh,M., Clark,K., Karsch-Mizrachi,I., Lipman,D.J., Ostell,J. and Sayers,E.W. (2013) GenBank. *Nucleic Acids Res.*, **41**, D36–42.

19. Schulz,M.H., Zerbino,D.R., Vingron,M. and Birney,E. (2012) Oases: robust de novo RNA-seq assembly across the dynamic range of expression levels. *Bioinformatics*, **28**, 1086–1092.

20. Grabherr,M.G., Haas,B.J., Yassour,M., Levin,J.Z., Thompson,D.A., Amit,I., Adiconis,X., Fan,L., Raychowdhury,R., Zeng,Q., *et al.* (2011) Full-length transcriptome assembly from RNA-Seq data without a reference genome. *Nat. Biotechnol.*, **29**, 644–652.

21. Cock,P.J.A., Chilton,J.M., Grüning,B., Johnson,J.E. and Soranzo,N. (2015) NCBI BLAST+ integrated into Galaxy. *Gigascience*, **4**, 39.

22. Camacho,C., Coulouris,G., Avagyan,V., Ma,N., Papadopoulos,J., Bealer,K. and Madden,T.L. (2009) BLAST+: architecture and applications. *BMC Bioinformatics*, **10**, 421.

23. Huang,X. and Madan,A. (1999) CAP3: A DNA sequence assembly program. *Genome Res.*, **9**, 868–877.

24. Titus Brown,C., Howe,A., Zhang,Q., Pyrkosz,A.B. and Brom,T.H. (2012) A Reference-Free Algorithm for Computational Normalization of Shotgun Sequencing Data. *arXiv [q-bio.GN]*.

25. Yozwiak,N.L., Skewes-Cox,P., Stenglein,M.D., Balmaseda,A., Harris,E. and DeRisi,J.L. (2012) Virus identification in unknown tropical febrile illness cases using deep sequencing. *PLoS Negl. Trop. Dis.*, **6**, e1485.

26. Kløverpris,H.N., Kazer,S.W., Mjösberg,J., Mabuka,J.M., Wellmann,A., Ndhlovu,Z., Yadon,M.C., Nhamoyebonde,S., Muenchhoff,M., Simoni,Y., *et al.* (2016) Innate Lymphoid Cells Are Depleted Irreversibly during Acute HIV-1 Infection in the Absence of Viral Suppression. *Immunity*, **44**, 391–405.

27. Matranga,C.B., Andersen,K.G., Winnicki,S., Busby,M., Gladden,A.D., Tewhey,R., Stremlau,M., Berlin,A., Gire,S.K., England,E., *et al.* (2014) Enhanced methods for unbiased deep sequencing of Lassa and Ebola RNA viruses from clinical and biological samples. *Genome Biol.*, **15**, 1–12.

28. Kim,M., Lee,K.-H., Yoon,S.-W., Kim,B.-S., Chun,J. and Yi,H. (2013) Analytical tools and databases for metagenomics in the next-generation sequencing era. *Genomics Inform.*, **11**, 102–113.

29. Caporaso,J.G., Kuczynski,J., Stombaugh,J., Bittinger,K., Bushman,F.D., Costello,E.K., Fierer,N., Peña,A.G., Goodrich,J.K., Gordon,J.I., *et al.* (2010) QIIME allows analysis of high-throughput community sequencing data. *Nat. Methods*, **7**, 335–336.

30. Quast,C., Pruesse,E., Yilmaz,P., Gerken,J., Schweer,T., Yarza,P., Peplies,J. and Glöckner,F.O. (2013) The SILVA ribosomal RNA gene database project: improved data processing and web-based tools. *Nucleic Acids Res.*, **41**, D590–6.

Legends to Figures

Figure 1. Global view of the Metavisitor workflow. The workflow is organised in sub workflows (dashed line) corresponding to functional tasks as described in the manuscript. All Galaxy Tools (square boxes) are available in the main Galaxy tool shed (https://toolshed.g2.bx.psu.edu/).

Figure 2. Realignments of small RNA sequence reads to reconstructed (Nora_MV, Nora_raw_reads and Nora_Median–Norm–reads) or published (JX220408.1 and NC_007919.3) Nora virus genomes. Plots (left) show the abundance of 18–30-nucleotide (nt) small RNA sequence reads matching the genome sequences and histograms (middle) show length distributions of these reads. Positive and negative values correspond to sense and antisense reads, respectively. Total read counts are indicated to the right hand side.

Legends to Tables

Table 1. Report table generated by the "Parse blast output and compile hits" tool in History for Use Case 1-4 showing the presence of *Drosophila* A virus and *Drosophila* C virus in addition to the Nora virus in the small RNA sequencing of laboratory *Drosophila*. See Method section for a description of the columns.

Table 2. HIV detection in RNA sequencing datasets from ILC patient samples. The table summarizes the report generated by Metavisitor from a batch of 40 sequence datasets using the Workflow for Use Case 3-1 in the Galaxy History for Use Case 3-1(dataset 199). This table reports the metadata associated with each indicated sequence dataset as well as the ability of Metavisitor to detect HIV in datasets and patients.

Table 3. Virus detection in RNAseq datasets from 36 traceable patients by Metavisitor after blast alignment of viral contigs (dataset 484 in Galaxy History for Use Case 3-2). For detection of false positives, reads were aligned to the bowtie2 vir1 index before de novo assembly (see dataset collection 261 in the history). The data from this computational treatment are summarized in the column "Read mapping to vir1 using bowtie2" and detailed in each corresponding patient tabs.

Table 4. Metavisitor detection of Lassa virus (55 RNAseq datasets) and of Ebola virus (8 RNAseq datasets). The table summarizes results obtained in the History for Use Case 3-3 Lassa L (dataset 566) and in the History for Use Case 3-3 Ebola (dataset 96). Reconstructed Lassa segment L and Ebola genome sequences are available in Galaxy dataset collections 679 and 115 of their respective histories.

Supplementary information

Supplementary Figure 1. Screenshot of an output produced by the "Parse blast output and compile hits" Metavisitor tool.

Supplementary File 1. MAFFT (http://www.ebi.ac.uk/Tools/msa/mafft/) Multiple Alignment of the Nora virus genome sequences published (JX220408.1 and NC_007919.3) or generated in Use Cases 1-1 to 1-3 (Nora_MV, Nora_raw_reads and Nora_Median–Norm–reads). A view of the alignments was produced by MView (http://www.ebi.ac.uk/Tools/msa/mview/). The html file can be visualized by opening it locally in any web browser software.

Figure 1

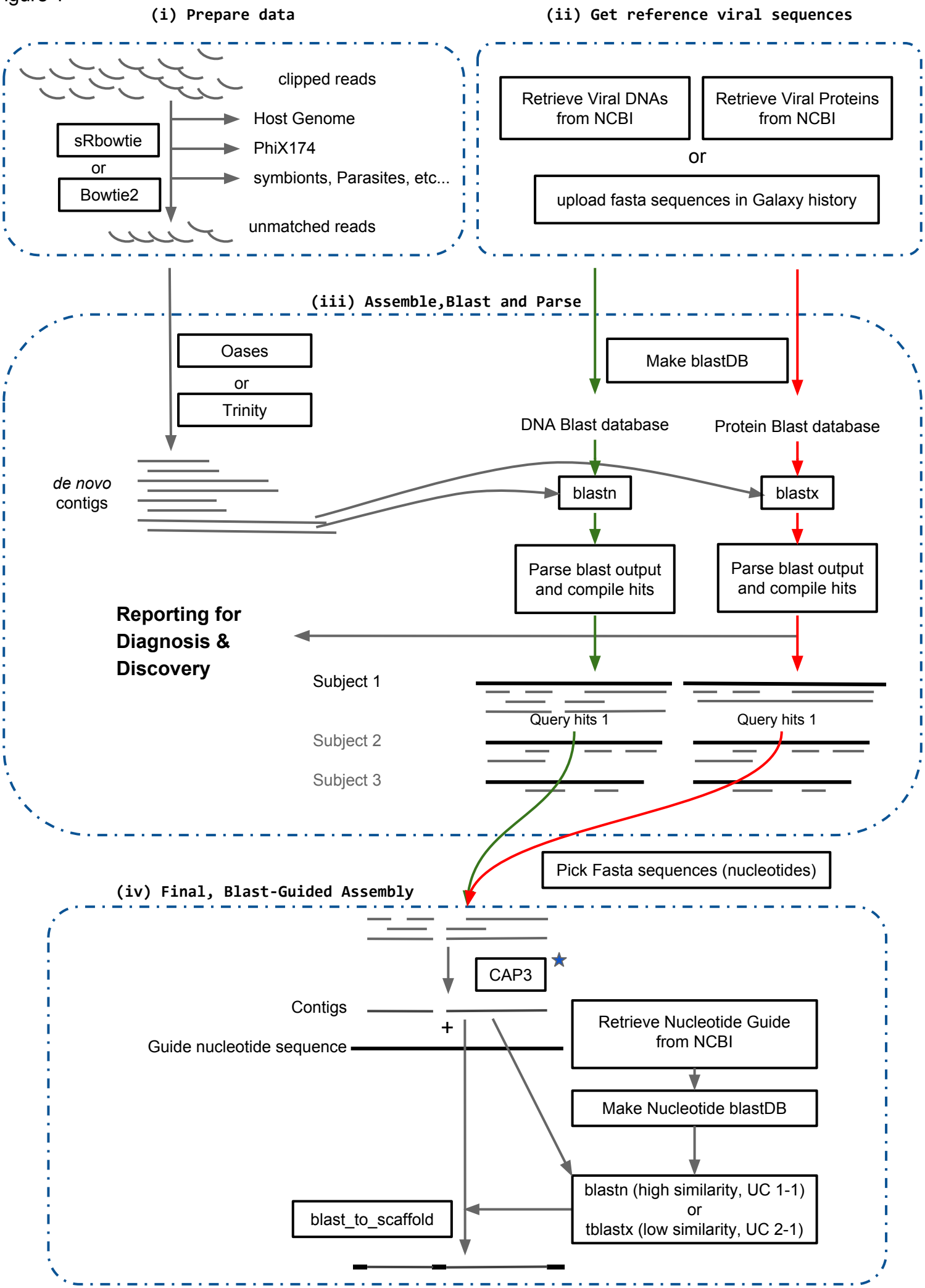

★ CAP3 assembly step is optional

Figure 2

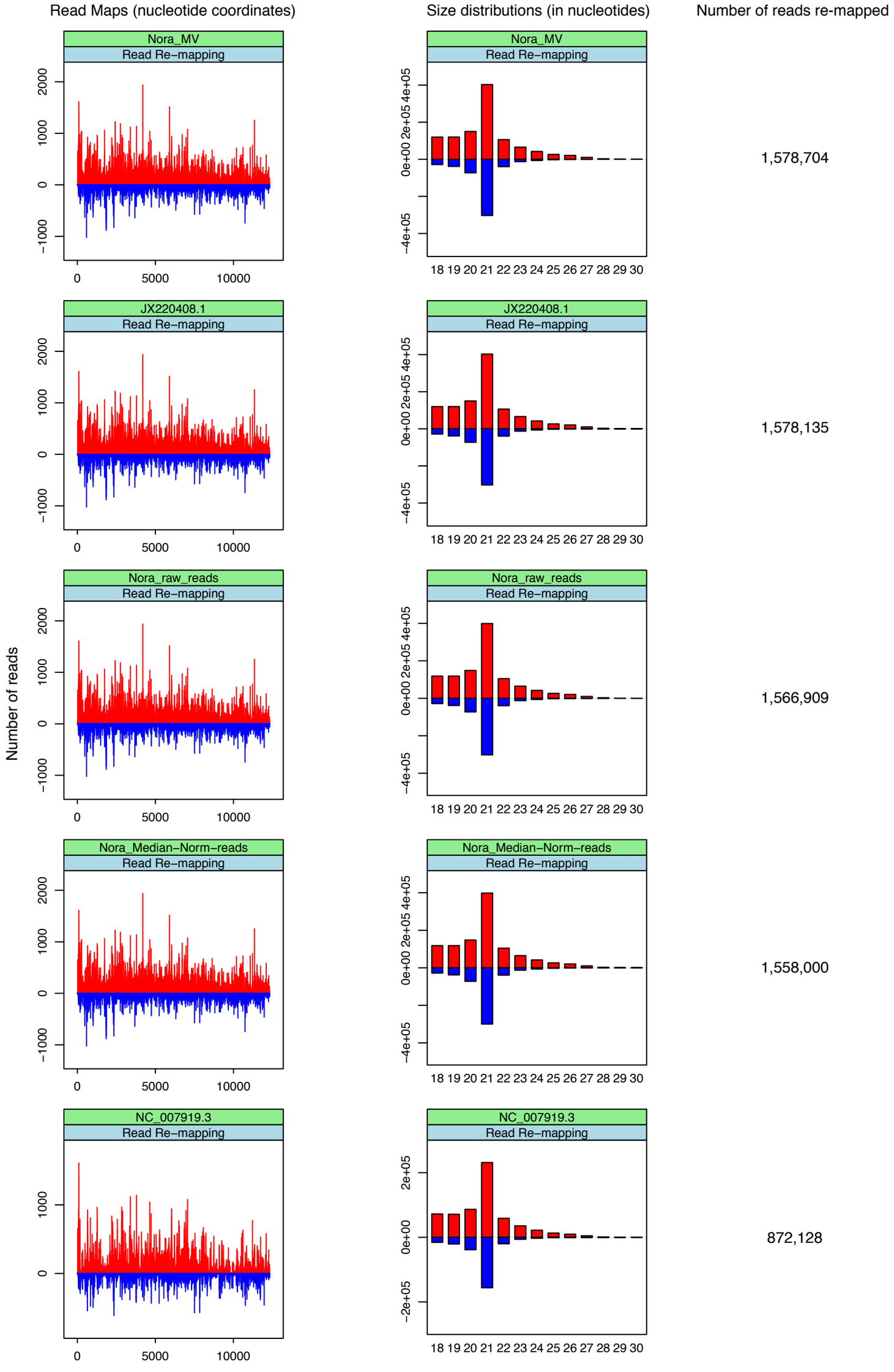
Read Maps (nucleotide coordinates)
Size distributions (in nucleotides)
Number of reads re-mapped
Nora_MV
Read Re−mapping
1,578,704
JX220408.1
Read Re−mapping
1,578,135
Nora_raw_reads
Read Re−mapping
1,566,909
Nora_Median−Norm−reads
Read Re−mapping
1,558,000
NC_007919.3
Read Re−mapping
872,128
Number of reads
0
5000
10000
18 19 20 21 22 23 24 25 26 27 28 29 30

Table 1

subject	subject length	Total Subject Coverage	Relative Subject Coverag	Best Bit Score	Mean Bit Score
gi|157325505|gb|DQ321720.2|_Nora_virus,_complete_genome	11908	10211	0.857490762513	11840.0	4041.13333333
gi|822478532|gb|KP970099.1|_Nora_virus_isolate_RAKMEL13_gp1_(gp1)_gene,_partial_cds;_and_replicatio	11416	8736	0.765241765943	11441.0	3673.0
gi|822478537|gb|KP970100.1|_Nora_virus_isolate_GEO58_gp1_(gp1)_gene,_partial_cds;_and_replication_p	11416	2463	0.215749824807	4028.0	3607.0
gi|346421290|ref|NC_007919.3|_Nora_virus,_complete_genome	12333	10530	0.853806859645	11809.0	2652.72727273
gi|284022350|gb|GQ257737.1|_Nora_virus_isolate_Umea_2007,_complete_genome	12333	10530	0.853806859645	11809.0	01/06/2572
gi|822478527|gb|KP970098.1|_Nora_virus_isolate_AM04_gp1_(gp1)_gene,_partial_cds;_and_replication_po	11413	7654	0.67063874529	5745.0	2488.72727273
gi|822478512|gb|KP970095.1|_Nora_virus_isolate_RAK11_gp1_(gp1)_and_replication_polyprotein_(gp2)_ge	11416	6174	0.540819901892	5368.0	01/02/2419
gi|822478141|gb|KP969947.1|_Drosophila_A_virus_isolate_ywiP_DrosophilaA_RNA-dependent_RNA_polymeras	4516	4157	0.920504871568	6980.0	2360.75
gi|402295620|gb|JX220408.1|_Nora_virus_isolate_FR1,_complete_genome	12333	12302	0.997486418552	12720.0	2324.48
gi|822478147|gb|KP969949.1|_Drosophila_A_virus_isolate_delta11_DrosophilaA_RNA-dependent_RNA_polyme	4481	4442	0.991296585584	7081.0	01/08/2263
gi|822478417|gb|KP970078.1|_Nora_virus_isolate_D167_gp1_(gp1),_replication_polyprotein_(gp2),_gp3_(	11895	7315	0.614964270702	5503.0	01/05/2191
gi|822478517|gb|KP970096.1|_Nora_virus_isolate_K09_gp1_(gp1)_gene,_partial_cds;_and_replication_pol	11419	2027	0.177511165601	3490.0	2050.0
gi|822478144|gb|KP969948.1|_Drosophila_A_virus_isolate_XIB_DrosophilaA_RNA-dependent_RNA_polymerase	4516	4507	0.998007085917	7092.0	01/05/2008
gi|822478150|gb|KP969950.1|_Drosophila_A_virus_isolate_Qdelta_DrosophilaA_RNA-dependent_RNA_polymer	4476	4446	0.993297587131	7092.0	1846.61538462
gi|822478440|gb|KP970082.1|_Nora_virus_isolate_RAKMEL12_gp1_(gp1),_replication_polyprotein_(gp2),_g	11968	7214	0.602774064171	6396.0	1815.36
gi|822478497|gb|KP970092.1|_Nora_virus_isolate_delta11_gp1_(gp1)_gene,_partial_cds;_replication_pol	11157	2347	0.21036120821	3314.0	1695.0
gi|822478522|gb|KP970097.1|_Nora_virus_isolate_JJ17_gp1_(gp1)_gene,_partial_cds;_and_replication_po	11420	993	0.0869527145359	1674.0	1659.0
gi|822478482|gb|KP970089.1|_Nora_virus_isolate_IM13_gp1_(gp1)_gene,_partial_cds;_replication_polypr	11103	1828	0.164640187337	1977.0	1565.0
gi|225356593|gb|FJ150422.1|_Drosophila_A_virus_isolate_HD,_complete_genome	4806	4753	0.988972118186	6902.0	1419.0
gi|822478430|gb|KP970080.1|_Nora_virus_isolate_MONSIM03_gp1_(gp1),_replication_polyprotein_(gp2),_g	11968	2086	0.174298128342	2993.0	01/04/1416
gi|822478445|gb|KP970083.1|_Nora_virus_isolate_SAF04_gp1_(gp1),_replication_polyprotein_(gp2),_gp3_	11142	649	0.0582480703644	1121.0	1121.0
gi|822478135|gb|KP969945.1|_Drosophila_A_virus_isolate_XID_DrosophilaA_RNA-dependent_RNA_polymerase	4516	4074	0.902125775022	3103.0	1111.55714286
gi|822478403|gb|KP970076.1|_Nora_virus_isolate_ATH56_gp1_(gp1)_and_replication_polyprotein_(gp2)_ge	11965	2344	0.195904722106	2812.0	01/05/1024
gi|822478412|gb|KP970077.1|_Nora_virus_isolate_IM09_gp1_(gp1),_replication_polyprotein_(gp2),_gp3_(	11965	3689	0.308315921438	2989.0	1023.28571429
gi|822478435|gb|KP970081.1|_Nora_virus_isolate_MON28_gp1_(gp1)_and_replication_polyprotein_(gp2)_ge	11967	5859	0.489596390073	5445.0	1003.92307692
gi|822478507|gb|KP970094.1|_Nora_virus_isolate_K02_gp1_(gp1)_gene,_partial_cds;_replication_polypro	11160	1289	0.115501792115	957.0	778.0
gi|822478132|gb|KP969944.1|_Drosophila_A_virus_isolate_wipe_DrosophilaA_RNA-dependent_RNA_polymeras	4516	3070	0.67980513729	3097.0	742.436363636
gi|822478477|gb|KP970088.1|_Nora_virus_isolate_IM12_gp1_(gp1)_gene,_partial_cds;_replication_polypr	11413	952	0.0834136510996	1153.0	732.333333333
gi|253761971|ref|NC_012958.1|_Drosophila_A_virus,_complete_genome	4806	607	0.126300457761	1045.0	674.2
gi|822478542|gb|KP970101.1|_Nora_virus_isolate_SAFSIM01_gp1_(gp1)_gene,_partial_cds;_and_replicatio	11413	384	0.0336458424604	661.0	661.0
gi|822478138|gb|KP969946.1|_Drosophila_A_virus_isolate_LJ35_DrosophilaA_RNA-dependent_RNA_polymeras	4468	959	0.214637421665	848.0	501.833333333
gi|9629650|ref|NC_001834.1|_Drosophila_C_virus,_complete_genome	9264	6345	0.684909326425	1276.0	444.609756098
gi|2388672|gb|AF014388.1|_Drosophila_C_virus_strain_EB,_complete_genome	9264	6587	0.711031951641	1276.0	431.272727273
gi|300871949|gb|GU983882.2|_Drosophila_C_virus_isolate_ZW141_polyprotein_gene,_partial_cds	500	272	0.544	482.0	394.5
gi|300871965|gb|GU983892.2|_Drosophila_C_virus_isolate_psjmg_polyprotein_gene,_partial_cds	500	310	0.62	491.0	352.75
gi|300871979|gb|GU983900.2|_Drosophila_C_virus_isolate_AL7_polyprotein_gene,_partial_cds	500	271	0.542	489.0	342.0

gi|300871957|gb|GU983888.2|_Drosophila_C_virus_isolate_Bam73_H_polyprotein_gene,_partial_cds	500	453	0.906	491.0	322.5
gi|300871941|gb|GU983878.2|_Drosophila_C_virus_isolate_mel15_H_polyprotein_gene,_partial_cds	500	453	0.906	489.0	321.0
gi|300871955|gb|GU983885.2|_Drosophila_C_virus_isolate_16a9_polyprotein_gene,_partial_cds	490	151	0.308163265306	273.0	262.0
gi|300871953|gb|GU983884.2|_Drosophila_C_virus_isolate_Tam15_polyprotein_gene,_partial_cds	500	151	0.302	273.0	262.0
gi|6940537|gb|AF065756.1|AF065756_Stealth_virus_1_clone_3B43_T7	836	599	0.716507177033	334.0	189.944444444
gi|6561412|gb|AF191073.1|AF191073_Stealth_virus_1_clone_3B43,_genomic_sequence	3620	2744	0.758011049724	432.0	182.938461538
gi|822478153|gb|KP969951.1|_Drosophila_A_virus_isolate_REEF23_DrosophilaA_RNA-dependent_RNA_polymer	468	125	0.267094017094	208.0	179.0
gi|6957471|gb|AF065755.1|AF065755_Stealth_virus_1_clone_3B43_T3	814	646	0.793611793612	279.0	174.709677419
gi|30014277|dbj|BD177017.1|_Novel_translational_activity-promoting_higher-order_structure	189	84	0.444444444444	152.0	152.0
gi|92142564|dbj|BD294721.1|_Novel_tertiary_structure_having_ability_to_accelerate_translation_activ	189	84	0.444444444444	152.0	152.0
gi|28414844|dbj|BD173513.1|_WO_2002061080-A/3:_Novel_tertiary_structure_having_ability_to_accelerat	189	84	0.444444444444	152.0	152.0
gi|767766613|gb|KM972720.1|_Tete_virus_strain_SaAn_3518_glycoprotein_precursor,_gene,_complete_cds	4467	115	0.0257443474368	156.0	148.5
gi|429890933|gb|JX904130.1|_Uncultured_marine_virus_clone_SOG02701,_complete_genome	1326	103	0.077677224736	145.0	142.333333333
gi|38569384|gb|AY397620.1|_Bluetongue_virus_isolate_10_5'_UTR	290	209	0.720689655172	223.0	140.169230769
gi|404515565|gb|JX291540.1|_Trichoderma_hypovirus_strain_1_clone_1_hypothetical_protein_gene,_compl	1923	132	0.0686427457098	174.0	127.755555556
gi|798547302|gb|KP974707.1|_Cricket_paralysis_virus_isolate_CrPV-3,_complete_genome	9185	908	0.098856831791	145.0	122.7
gi|798547249|gb|KP974706.1|_Cricket_paralysis_virus_isolate_CrPV-2,_complete_genome	9381	2108	0.224709519241	167.0	114.128571429
gi|8895506|gb|AF218039.1|_Cricket_paralysis_virus_nonstructural_polyprotein_and_structural_polyprot	9185	1871	0.203701687534	167.0	112.716666667
gi|21321708|ref|NC_003924.1|_Cricket_paralysis_virus,_complete_genome	9185	1411	0.153620032662	167.0	107.95
gi|331693811|gb|HQ442266.1|_Grapevine_leafroll-associated_virus_1_isolate_12.2.1_coat_protein-like_	544	128	0.235294117647	107.0	107.0
gi|236164896|emb|GN351224.1|_Sequence_988_from_Patent_WO2007130519	60	60	1.0	104.0	104.0
gi|236164898|emb|GN351225.1|_Sequence_989_from_Patent_WO2007130519	60	60	1.0	104.0	104.0
gi|236164921|emb|GN351233.1|_Sequence_997_from_Patent_WO2007130519	60	60	1.0	100.0	100.0
gi|236164917|emb|GN351232.1|_Sequence_996_from_Patent_WO2007130519	60	60	1.0	100.0	100.0
gi|567840469|gb|KF478765.1|_Lassa_virus_strain_Soromba-R_segment_S,_complete_sequence	3571	145	0.0406048725847	104.0	93.2875
gi|399157421|gb|JX185667.1|_UNVERIFIED:_Deformed_wing_virus_clone_100414-13_L20_16D-DWV1F_A1_pol	941	183	0.194473963868	109.0	90.2
gi|399157420|gb|JX185666.1|_UNVERIFIED:_Deformed_wing_virus_clone_100414-13_K20_15D-DWV1F_A1_pol	942	183	0.194267515924	109.0	89.6571428571
gi|399157416|gb|JX185662.1|_UNVERIFIED:_Deformed_wing_virus_clone_100414-13_O19_8D-DWV1F_A1_poly	947	183	0.193241816262	100.0	85.4714285714
gi|399157417|gb|JX185663.1|_UNVERIFIED:_Deformed_wing_virus_clone_100414-13_P19_10D-DWV1F_A1_pol	944	183	0.193855932203	100.0	82.9
gi|822478059|gb|KP969918.1|_Drosophila_A_virus_isolate_IM13_DrosophilaA_RNA-dependent_RNA_polymeras	4480	60	0.0133928571429	100.0	82.2
gi|84683224|gb|DQ333351.1|_Choristoneura_occidentalis_granulovirus,_complete_genome	104710	77	0.000735364339605	104.0	78.8428571429
gi|109255272|ref|NC_008168.1|_Choristoneura_occidentalis_granulovirus,_complete_genome	104710	77	0.000735364339605	104.0	78.8428571429
gi|726973360|gb|KM270560.1|_Nilaparvata_lugens_C_virus,_complete_genome	9163	791	0.0863254392666	174.0	77.3777777778
gi|766989358|gb|KP642119.1|_Narnaviridae_environmental_sample_clone_sraf.cpip_contig2643_RNA-depend	3246	86	0.026494146642	75.2	75.2
gi|236164892|emb|GN351222.1|_Sequence_986_from_Patent_WO2007130519	60	44	0.733333333333	75.2	75.2
gi|399157419|gb|JX185665.1|_UNVERIFIED:_Deformed_wing_virus_clone_100414-13_J20_13D-DWV1F_A1_pol	657	103	0.156773211568	89.7	74.575
gi|346450872|emb|JA417780.1|_Sequence_2_from_Patent_WO2011075379	7159	47	0.00656516273223	71.6	71.6

gi|262225307|gb|GQ342964.1|_Drosophila_melanogaster_tetravirus_SW-2009a_strain_DTRV_putative_RNA-de	3005	41	0.0136439267887	69.8	69.8
gi|84579786|dbj|AB214978.1|_Human_picobirnavirus_pseudogene_for_RNA-dependent_RNA_polymerase	193	137	0.709844559585	95.1	69.1
gi|254575700|gb|FJ539167.1|_Oxbow_virus_strain_Ng1453_glycoprotein_gene,_complete_cds	3643	36	0.00988196541312	66.2	66.2
gi|822478117|gb|KP969939.1|_Drosophila_A_virus_isolate_IM08_DrosophilaA_RNA-dependent_RNA_polymeras	4503	35	0.00777259604708	64.4	64.4
gi|822478120|gb|KP969940.1|_Drosophila_A_virus_isolate_IM02_DrosophilaA_RNA-dependent_RNA_polymeras	4480	35	0.0078125	64.4	64.4
gi|723005622|gb|KM382272.1|_Bat_circovirus_POA/2012/V,_partial_genome	1728	56	0.0324074074074	64.4	64.04
gi|609088848|gb|KJ191556.1|_Baku_virus_strain_LEIV-46Azn_VP5_protein_gene,_partial_cds	1620	40	0.0246913580247	64.4	58.7
gi|401772014|emb|HE795107.1|_Shamonda_virus_N_and_NSs_genes,_segment_S,_genomic_RNA,_isolate_Ib_	927	32	0.0345199568501	53.6	53.0
gi|401829616|ref|NC_018464.1|_Shamonda_virus_N_and_NSs_genes,_segment_S,_genomic_RNA,_isolate_Ib_A	927	32	0.0345199568501	53.6	52.7
gi|767851454|gb|KJ936089.1|_Turnip_mosaic_virus_isolate_NSW3,_complete_genome	9834	51	0.00518608907871	51.8	51.8
gi|187234321|gb|EU436423.1|_Israel_acute_paralysis_virus_of_bees_strain_DVE31-OP3-PA-USA-2007,_comp	9580	82	0.00855949895616	50.0	50.0

Table 2

Metavisitor HIV detection (last two columns)

# GSM ID	ID-1	Patient	Treatment (SRR annotations)	HIV status	Days post HIV infection	Treatment status	SRR ID	Metavisitor HIV detection by sample	number of raw reads	number of raw reads by patient	History for Use Case 3-1
GSM2043730	110314	0450-318	ILC2	HIV+	1	untreated	SRR3111582	+	7 013 962	34 252 732	gi|45357423|gb|AY535449.1 gi|45357419|gb|AY535447.1
GSM2043731	110314	0450-318	ILC3	HIV+	1	untreated	SRR3111583	-	3 246 980		
GSM2043732	180314	0450-318	ILC2	HIV+	7	untreated	SRR3111584	+	2 833 634		
GSM2043733	180314	0450-318	ILC3	HIV+	7	untreated	SRR3111585	+	2 989 628		
GSM2043734	170414	0450-318	ILC2	HIV+	38	untreated	SRR3111586	-	16 248 912		
GSM2043735	170414	0450-318	ILC3	HIV+	38	untreated	SRR3111587	-	1 919 616		
GSM2043736	110614	0387-272	ILC2	HIV+	1	untreated	SRR3111588	-	60 342 796	227 307 414	-
GSM2043737	110614	0387-272	ILC3	HIV+	1	untreated	SRR3111589	-	34 189 278		
GSM2043738	170614	0387-272	ILC2	HIV+	7	untreated	SRR3111590	-	38 030 394		
GSM2043739	170614	0387-272	ILC3	HIV+	7	untreated	SRR3111591	-	29 100 534		
GSM2043740	290714	0387-272	ILC2	HIV+	49	untreated	SRR3111592	-	43 022 506		
GSM2043741	290714	0387-272	ILC3	HIV+	49	untreated	SRR3111593	-	22 621 906		
GSM2043742	41214	0629-453	Acute ART+ ILC2	HIV+	1	ART	SRR3111594	+	5 061 920	54 052 098	gi|296033826|gb|GU474419.1 gi|269294806|dbj|DM461231.1 gi|269294805|dbj|DM461230.1 gi|296556482|gb|AF324493.2 gi|296556485|gb|M19921.2 gi|45357419|gb|AY535447.1 gi|45357423|gb|AY535449.1
GSM2043743	41214	0629-453	Acute ART+ ILC3	HIV+	1	ART	SRR3111595	-	8 455 026		
GSM2043744	101214	0629-453	Acute ART+ ILC2	HIV+	6	ART	SRR3111596	-	12 451 684		
GSM2043745	101214	0629-453	Acute ART+ ILC3	HIV+	6	ART	SRR3111597	+	6 419 868		
GSM2043746	130115	0629-453	Acute ILC2	HIV+	40	ART	SRR3111598	+	6 837 584		
GSM2043747	130115	0629-453	Acute ILC3	HIV+	40	ART	SRR3111599	+	14 826 016		
GSM2043748	150714	0444-312	3dR10 ILC2	HIV+	2	ART	SRR3111600	+	15 618 282	39 610 902	gi|45357423|gb|AY535449.1 gi|45357419|gb|AY535447.1
GSM2043749	150714	0444-312	3dR10 ILC3	HIV+	2	ART	SRR3111601	+	13 491 804		
GSM2043750	220814	0444-312	ILC2	HIV+	41	ART	SRR3111602	-	5 259 104		
GSM2043751	220814	0444-312	ILC3	HIV+	41	ART	SRR3111603	-	5 241 712		
GSM2043752	10814	0500-355neg	ILC2	HIV-	uninfected	none	SRR3111604	-	802 632	11 691 304	-
GSM2043753	10814	0500-355neg	ILC3	HIV-	uninfected	none	SRR3111605	-	10 888 672		
GSM2043754	80814	0292-xxxneg	ILC2	HIV-	uninfected	none	SRR3111606	-	5 418 958	19 222 152	-
GSM2043755	80814	0292-xxxneg	ILC3	HIV-	uninfected	none	SRR3111607	-	13 803 194		
GSM2043756	90714	0394-274	ILC2	HIV-	uninfected	none	SRR3111608	-	13 779 570	15 991 428	-
GSM2043757	90714	0394-274	ILC3	HIV-	uninfected	none	SRR3111609	-	2 211 858		
GSM2043758	170714	0218-162neg	ILC2	HIV-	uninfected	none	SRR3111610	-	9 838 776	18 939 560	- (gi|6940537|gb|AF065756.1|AF065756_Stealth_virus_1_clone_3B43_T7)
GSM2043759	170714	0218-162neg	ILC3	HIV-	uninfected	none	SRR3111611	-	9 100 784		
GSM2043760	180314	0311-217HIVneg	ILC2	HIV-	uninfected	none	SRR3111612	-	2 281 560	7 490 832	- (gi|6940537|gb|AF065756.1|AF065756_Stealth_virus_1_clone_3B43_T7)
GSM2043761	180314	0311-217HIVneg	ILC3	HIV-	uninfected	none	SRR3111613	-	5 209 272		
GSM2043762	230514	0440-307neg	ILC2	HIV-	uninfected	none	SRR3111614	-	11 816 186	21 714 164	-
GSM2043763	230514	0440-307neg	ILC3	HIV-	uninfected	none	SRR3111616	-	9 897 978		
GSM2043764	240614	0518-370neg	ILC2	HIV-	uninfected	none	SRR3111617	-	16 135 602	16 671 200	- (gi|6940537|gb|AF065756.1|AF065756_Stealth_virus_1_clone_3B43_T7)
GSM2043765	240614	0518-370neg	ILC3	HIV-	uninfected	none	SRR3111618	-	535 598		
GSM2043766	290714	0560-420neg	ILC2	HIV-	uninfected	none	SRR3111619	-	1 235 766	12 912 002	- (gi|6940537|gb|AF065756.1|AF065756_Stealth_virus_1_clone_3B43_T7)
GSM2043767	290714	0560-420neg	ILC3	HIV-	uninfected	none	SRR3111620	-	11 676 236		
GSM2043768	290714	0575-419neg	ILC2	HIV-	uninfected	none	SRR3111621	-	8 713 816	11 833 416	- (gi|6940537|gb|AF065756.1|AF065756_Stealth_virus_1_clone_3B43_T7)
GSM2043769	290714	0575-419neg	ILC3	HIV-	uninfected	none	SRR3111622	-	3 119 600		

Table 3

Extracted from Yozwiak et al. Table 1					Metavisitor			
Patient ID	**# virus reads**	**# initial reads**	**Fraction virus reads**	**Yozwiak et al. Virus detection**	**# reads in NGS datasets**	**Metavisitor Virus detection**	**Read mapping to vir1 using bowtie2**	**ENA-RUN**
566	206	1,90E+06	1,08E-04	Torque teno mini virus 4	1,07E+06	none	No Significant alignments	SRR453487
438	72	4,40E+06	1,64E-05	Human herpesvirus 6	3,20E+06	Human herpesvirus 6	49 Human_herpesvirus_6	SRR453437
401	2164	1,80E+05	1,20E-02	Hepatitis A virus	9,94E+05	Hepatitis A virus	6154 reads Hepatitis_A_virus,	SRR453443,SRR453458
382	44	9,60E+05	4,58E-05	Human herpesvirus 4	2,33E+06	none	38 Human_herpesvirus_4	SRR453430
377	81	6,60E+06	1,23E-05	Cyclovirus PK5034	4,91E+06	Circovirus-like_NI/2007-3	58 reads Circovirus-like_NI/2007-3 76 Torque teno virus	SRR453491
375	53	3,80E+06	1,39E-05	Porcine circovirus 1	2,65E+06	Circovirus-like_NI/2007-3	66 reads Circovirus-like_NI/2007-3	SRR453499
350	48	3,00E+06	1,60E-05	Human herpesvirus 6, Torque teno mini virus 4	1,93E+06	none	29 Human_herpesvirus_6 128 Torque teno mini virus 4	SRR453484
349	47	1,60E+06	2,94E-05	Torque teno midi virus	1,03E+06	none	No Significant alignments	SRR453464
345	62	2,20E+06	2,82E-05	Beak and feather disease virus	1,29E+06	Dengue_virus_4	159 Dengue_virus_4 65 Circovirus-like_NI/2007	SRR453506
344	303	1,30E+06	2,33E-04	Human herpesvirus 6	7,48E+05	Human herpesvirus 6	184 Human_herpesvirus_6	SRR453417
335	47	1,70E+06	2,76E-05	Torque teno virus	9,77E+05	none	24 Torque teno virus	SRR453490
331	113	1,40E+06	8,07E-05	Torque teno midi virus 2	8,99E+05	UNVERIFIED:_Torque_teno_virus_isolate_S55,_complete_genome	772 Torque teno virus	SRR453478
330	77	1,80E+06	4,28E-05	TTV-like mini virus	1,85E+06	AF191073_Stealth_virus_1_clone_3B43	14 reads Stealth_virus_1_clone_C16130_T3 24 reads Dengue virus 2	SRR453465,SRR453480
329	14	2,20E+06	6,36E-06	Gull circovirus	2,93E+06	Circovirus-like_NI/2007-3	5 reads Circovirus-like_NI/2007-3 12 reads Dengue virus 2	SRR453489,SRR453505
322	206	3,80E+06	5,42E-05	Cyclovirus PK5222	2,63E+06	Circovirus-like_NI/2007-3	208 reads Circovirus-like_NI/2007-3	SRR453498
321	30	4,60E+06	6,52E-06	Porcine circovirus 1	3,54E+06	none	10 reads Circovirus-like_NI/2007-3 17 reads Dengue virus 2	SRR453446
315	42	1,90E+06	2,21E-05	African swine fever virus	1,59E+06	none	22 reads Dengue virus 2	SRR453427,SRR453440
282	699	1,60E+06	4,20E-04	Dengue virus 2	9,66E+05	Dengue virus 2	651 reads Dengue virus 2	SRR453438
275	1511	1,60E+06	9,70E-04	Dengue virus 2	1,11E+06	Dengue virus 2	1436 reads Dengue virus 2	SRR453450
274	27	1,20E+06	2,30E-05	Dengue virus 1	6,24E+05	none	28 reads Dengue virus 1/2	SRR453460
270	28	1,20E+06	2,33E-05	Human herpesvirus 6	6,76E+05	none	20 Human_herpesvirus_6	SRR453485
266	135749	4,80E+06	2,80E-02	Dengue virus 2	3,36E+06	Dengue virus 2	121347 reads Dengue virus 2	SRR453448
263	ND	ND	ND	TTV (virochip)	3142332	Dengue virus 2	75 densovirus 92 Dengue virus	SRR453424,SRR453457
193	56	1,60E+06	3,50E-05	Torque teno mini virus 2	9,13E+05	none	6 reads Torque_teno_virus_isolate_TTV-S34	SRR453510
187	4280	1,10E+06	3,90E-03	Dengue virus 2	5,55E+05	Dengue virus 2	3970 reads Dengue virus 2	SRR453456
186	1701	2,00E+06	8,51E-04	Torque teno virus 15	1,32E+06	Torque teno virus (SEN virus)	541 SEN virus AY449524.1 27 reads Torque_teno_virus_15	SRR453425,SRR453469
183	66	3,00E+06	2,20E-05	Human herpesvirus 6	1,97E+06	none	57 Human_herpesvirus_6B	SRR453481
180	42	8,00E+05	5,25E-05	GB virus C	4,91E+06	GB virus C	41 reads GB virus	SRR453531
179	17	1,80E+06	9,44E-06	Torque teno mini virus 1	1,31E+06	none	No Significant alignments	SRR453474
171	18	1,20E+06	1,50E-05	Torque teno mini virus 2	7,81E+05	none	No Significant alignments	SRR453509
168	ND	ND	ND	TTV (virochip)	135412	none	No Significant alignments	SRR453451
161	14	3,00E+06	4,67E-06	Human parvovirus B19	2,75E+06	Human parvovirus B19	79 densovirus 12 reads Human parvovirus B19	SRR453495,SRR453504
159	143	2,60E+06	5,50E-05	Torque teno mini virus 5	1,73E+06	none	No Significant alignments	SRR453500
156	213	2,30E+06	9,26E-05	Torque teno midi virus 1	1,54E+06	Torque_teno_virus	550 reads Torque_teno_virus_isolate_S54	SRR453493
131	24	1,20E+06	2,00E-05	Human herpesvirus 6	5,46E+05	Human herpesvirus 6	16 reads Human_herpesvirus_6	SRR453444
78	113	1,20E+06	9,42E-05	Human herpesvirus 6	5,91E+05	none	68 reads Human_herpesvirus_6B	SRR453426

Table 4

Virus	BioProject	BioSample id	SRX number	SRR number	Sample ID	BAM file name	Source	Data Type, Selection	Figure, Table from Matranga *et al.*	Metavisitor detection (Trinity)
EBOV	PRJNA257197	SAMN03099684	SRX733660	SRR1613381	G3676-2	G3676-2_S6_L001_001.bam	Human	RNase H	Figure 5	+
EBOV	PRJNA257197	SAMN03099684	SRX733656	SRR1613377	G3676-2	G3676-2-std_S13_L001_001.bam	Human	RNA seq	Figure 5	+
EBOV	PRJNA257197	SAMN03099685	SRX733661	SRR1613382	G3677-1	G3677-1_S3_L001_001.bam	Human	RNase H	Figure 5	+
EBOV	PRJNA257197	SAMN03099685	SRX733657	SRR1613378	G3677-1	G3677-1-std_S10_L001_001.bam	Human	RNA seq	Figure 5	+
EBOV	PRJNA257197	SAMN03099686	SRX733662	SRR1613383	G3677-2	G3677-2_S2_L001_001.bam	Human	RNase H	Figure 5	+
EBOV	PRJNA257197	SAMN03099686	SRX733658	SRR1613379	G3677-2	G3677-2-std_S9_L001_001.bam	Human	RNA seq	Figure 5	+
EBOV	PRJNA257197	SAMN03099687	SRX733663	SRR1613384	G3682-1	G3682-1_S4_L001_001.bam	Human	RNase H	Figure 5	+
EBOV	PRJNA257197	SAMN03099687	SRX733659	SRR1613380	G3682-1	G3682-1-std_S11_L001_001.bam	Human	RNA seq	Figure 5	+
LASV	PRJNA254017	SAMN02927412	SRX719120	SRR1595772	G2431	LASV678_ERCC117	Human	RNase H	Figure 2	+
LASV	PRJNA254017	SAMN02927412	SRX719079	SRR1595696	G2431	LASV678_ERCC12	Human	RNA seq	Figure 2	+
LASV	PRJNA254017	SAMN02927488	SRX719056	SRR1595665	ISTH1003	LASV347_ERCC126	Human	RNase H	Figure 2	+
LASV	PRJNA254017	SAMN02927488	SRX718926	SRR1595500	ISTH1003	LASV347_ERCC17	Human	RNA seq	Figure 2	+
LASV	PRJNA254017	SAMN02927485	SRX718761	SRR1594619	ISTH0531	LASV334_ERCC136	Human	RNase H	Figure 2	+
LASV	PRJNA254017	SAMN02927485	SRX719205	SRR1595943	ISTH0531	LASV334_ERCC31	Human	RNA seq	Figure 2	+
LASV	PRJNA254017	SAMN02927498	SRX719063	SRR1595673	ISTH1121	LASV363_ERCC69	Human	RNase H	Figure 2	+
LASV	PRJNA254017	SAMN02927498	SRX719134	SRR1595797	ISTH1121	LASV363_ERCC43	Human	RNA seq	Figure 2	+
LASV	PRJNA254017	SAMN02927489	SRX719117	SRR1595763	ISTH1038	LASV349_ERCC62	Human	RNase H	Figure 2	+
LASV	PRJNA254017	SAMN02927489	SRX718979	SRR1595558	ISTH1038	LASV349_ERCC42	Human	RNA seq	Figure 2	+
LASV	PRJNA254017	SAMN02927510	SRX718802	SRR1594664	ISTH2050	LASV386_ERCC84	Human	RNase H	Figure 2	+
LASV	PRJNA254017	SAMN02927503	SRX719192	SRR1595909	ISTH2020	LASV368_ERCC112	Human	RNase H	Figure 2	+
LASV	PRJNA254017	SAMN02927484	SRX718789	SRR1594651	ISTH0230	LASV435_ERCC96	Human	RNase H	Figure 2	+
LASV	PRJNA254017	SAMN02927592	SRX719159	SRR1595835	LM032.dep	LM032_Depleted	Mastomys	RNase H	Figure 3	+
LASV	PRJNA254017	SAMN02927592	SRX718836	SRR1594698	LM032.std	LM032_Standard	Mastomys	RNA seq	Figure 3	+
LASV	PRJNA254017	SAMN03099734	SRX733666	SRR1613388	NHP_DK9W-AG.dep	728_Depleted	Macaque	RNase H	Figure 3	+
LASV	PRJNA254017	SAMN03099735	SRX733667	SRR1613389	NHP_DK9W-AG.std	728_Standard	Macaque	RNA seq	Figure 3	+
LASV	PRJNA254017	SAMN03099736	SRX733668	SRR1613390	NHP_DK9W-AL.dep	729_Depleted	Macaque	RNase H	Figure 3	+
LASV	PRJNA254017	SAMN03099737	SRX733669	SRR1613391	NHP_DK9W-AL.std	729_Standard	Macaque	RNA seq	Figure 3	+
LASV	PRJNA254017	SAMN03099738	SRX733670	SRR1613392	NHP_DK9W-B.dep	734_Depleted	Macaque	RNase H	Figure 3	+
LASV	PRJNA254017	SAMN03099739	SRX733671	SRR1613393	NHP_DK9W-B.std	734_Standard	Macaque	RNA seq	Figure 3	+
LASV	PRJNA254017	SAMN03099740	SRX733672	SRR1613394	NHP_DK9W-K.dep	733_Depleted	Macaque	RNase H	Figure 3	+

LASV	PRJNA254017	SAMN03099741	SRX733673	SRR1613395	NHP_DK9W-K.std	733_Standard	Macaque	RNA seq	Figure 3	+
LASV	PRJNA254017	SAMN03099742	SRX733674	SRR1613396	NHP_DK9W-L.dep	731_Depleted	Macaque	RNase H	Figure 3	+
LASV	PRJNA254017	SAMN03099743	SRX733675	SRR1613397	NHP_DK9W-L.std	731_Standard	Macaque	RNA seq	Figure 3	+
LASV	PRJNA254017	SAMN03099744	SRX733676	SRR1613398	NHP_DK9W-S.dep	732_Depleted	Macaque	RNase H	Figure 3	+
LASV	PRJNA254017	SAMN03099745	SRX733677	SRR1613399	NHP_DK9W-S.std	732_Standard	Macaque	RNA seq	Figure 3	+
LASV	PRJNA254017	SAMN02927592	SRX719168	SRR1595853	LM032	LASV68_BLC	Mastomys	RNA seq	Figure 4, Table 1	+
LASV	PRJNA254017	SAMN02927476	SRX727329	SRR1606288	G733	LASV_90	Human	RNA seq	Figure 4, Table 1	+
LASV	PRJNA254017	SAMN02927592	SRX733690	SRR1613412	LM032	LM032_HS	Mastomys	Hybrid Selection	Figure 4, Table 1	+
LASV	PRJNA254017	SAMN02927476	SRX733681	SRR1613403	G733	G733_HS	Human	Hybrid Selection	Figure 4, Table 1	+
LASV	PRJNA254017	SAMN02927593	SRX727318	SRR1606277	LM222	LASV_74	Mastomys	RNA seq	Table 1	+
LASV	PRJNA254017	SAMN03099732	SRX733664	SRR1613386	Z002	LASV_77	Mastomys	RNA seq	Table 1	-
LASV	PRJNA254017	SAMN03099733	SRX733665	SRR1613387	G090	LASV_79	Human	RNA seq	Table 1	+
LASV	PRJNA254017	SAMN02927477	SRX727310	SRR1606267	G771	LASV94	Human	RNA seq	Table 1	+
LASV	PRJNA254017	SAMN02927399	SRX734464	SRR1614275	G2230	Solexa-100929.tagged_332	Human	RNA seq	Table 1	+
LASV	PRJNA254017	SAMN02927483	SRX731079	SRR1610580	ISTH0073	Solexa-106870.tagged_851	Human	RNA seq	Table 1	+
LASV	PRJNA254017	SAMN02927500	SRX719163	SRR1595846	ISTH1137	LASV353_BLC	Human	RNA seq	Table 1	+
LASV	PRJNA254017	SAMN02927503	SRX718749	SRR1594606	ISTH2020	LASV368_ERCC03	Human	RNA seq	Table 1	+
LASV	PRJNA254017	SAMN02927504	SRX727274	SRR1606236	ISTH2025	LASV374_ERCC58	Human	RNA seq	Table 1	+
LASV	PRJNA254017	SAMN02927510	SRX718860	SRR1594723	ISTH2050	LASV386_ERCC48	Human	RNA seq	Table 1	+
LASV	PRJNA254017	SAMN02927484	SRX718809	SRR1594671	ISTH0230	LASV435_ERCC53	Human	RNA seq	Table 1	+
LASV	PRJNA254017	SAMN02927593	SRX733692	SRR1613414	LM222	LM222_HS	Mastomys	Hybrid Selection	Table 1	+
LASV	PRJNA254017	SAMN03099732	SRX733678	SRR1613400	Z002	Z002_HS	Mastomys	Hybrid Selection	Table 1	+
LASV	PRJNA254017	SAMN03099733	SRX733679	SRR1613401	G090	G090_HS	Human	Hybrid Selection	Table 1	+
LASV	PRJNA254017	SAMN02927477	SRX733682	SRR1613404	G771	G771_HS	Human	Hybrid Selection	Table 1	+
LASV	PRJNA254017	SAMN02927399	SRX733680	SRR1613402	G2230	G2230_HS	Human	Hybrid Selection	Table 1	+
LASV	PRJNA254017	SAMN02927483	SRX733683	SRR1613405	ISTH0073	ISTH0073_HS	Human	Hybrid Selection	Table 1	+
LASV	PRJNA254017	SAMN02927500	SRX733685	SRR1613407	ISTH1137	ISTH1137_HS	Human	Hybrid Selection	Table 1	+
LASV	PRJNA254017	SAMN02927503	SRX733686	SRR1613408	ISTH2020	ISTH2020_HS	Human	Hybrid Selection	Table 1	+
LASV	PRJNA254017	SAMN02927504	SRX733687	SRR1613409	ISTH2025	ISTH2025_HS	Human	Hybrid Selection	Table 1	+
LASV	PRJNA254017	SAMN02927510	SRX733688	SRR1613410	ISTH2050	ISTH2050_HS	Human	Hybrid Selection	Table 1	+
LASV	PRJNA254017	SAMN02927484	SRX733684	SRR1613406	ISTH0230	ISTH0230_HS	Human	Hybrid Selection	Table 1	+
LASV	PRJNA254017	SAMN02927592	SRX733689	SRR1613411	LM032	LM032_Depleted	Mastomys	cDNA	ND, manually added to the original sup file 3	+
LASV	PRJNA254017	SAMN02927592	SRX733691	SRR1613413	LM032	LM032_Standard	Mastomys	cDNA	ND, manually added to the original sup file 3	-

1	2	3	4	5	6	7	8
# SeqId	%Identity	AlignLength	StartSubject	EndSubject	%QueryHitCov	E-value	BitScore
#							
# gi|157325505|gb|DQ321720.2|_Nora_virus,_complete_genome							
# Suject Length: 11908							
# Total Subject Coverage: 8338							
# Relative Subject Coverage: 0.70020154518							
# Best Bit Score: 10502.0							
# Mean Bit Score: 4066.30769231							
Locus_3_Transcript_33/33_Confidence_0.000_Length_1728	97.11	1730	11890	10161	99.9	0.0	2892.0
Locus_3_Transcript_3/33_Confidence_0.029_Length_1261	98.1	1261	6840	5580	99.9	0.0	2167.0
Locus_3_Transcript_2/33_Confidence_0.057_Length_1264	98.1	1261	6840	5580	99.7	0.0	2167.0
Locus_3_Transcript_31/33_Confidence_0.114_Length_3832	96.16	3724	11890	8167	97.1	0.0	6066.0
Locus_3_Transcript_31/33_Confidence_0.114_Length_3832	96.09	128	1807	1680	3.3	1e-50	208.0
Locus_3_Transcript_30/33_Confidence_0.171_Length_4066	96.26	4038	11890	7853	99.2	0.0	6596.0
Locus_3_Transcript_6/33_Confidence_0.057_Length_1925	97.66	1925	5605	3681	99.9	0.0	3268.0
Locus_3_Transcript_29/33_Confidence_0.171_Length_4089	96.24	4093	11890	7798	100.0	0.0	6682.0
Locus_3_Transcript_32/33_Confidence_0.057_Length_6307	96.93	6311	11890	5580	100.0	0.0	10502.0
Locus_3_Transcript_1/33_Confidence_0.057_Length_650	98.77	649	7463	6815	99.7	0.0	1135.0
Locus_3_Transcript_4/33_Confidence_0.086_Length_2045	98.18	2033	6840	4808	99.4	0.0	3499.0
Locus_3_Transcript_24/33_Confidence_0.086_Length_2244	98.22	2244	7823	5580	100.0	0.0	3867.0
Locus_3_Transcript_5/33_Confidence_0.086_Length_2212	98.24	2212	6840	4629	100.0	0.0	3813.0
#							
# gi|822478537|gb|KP970100.1|_Nora_virus_isolate_GEO58_gp1_(gp1)_gene,_partial_cds;_and_replication_p							
# Suject Length: 11416							
# Total Subject Coverage: 2463							
# Relative Subject Coverage: 0.215749824807							
# Best Bit Score: 4028.0							
# Mean Bit Score: 3607.0							
Locus_3_Transcript_22/33_Confidence_0.114_Length_2104	96.29	2105	9693	7589	100.0	0.0	3442.0
Locus_3_Transcript_23/33_Confidence_0.143_Length_2464	96.31	2463	9693	7231	99.9	0.0	4028.0
Locus_3_Transcript_20/33_Confidence_0.086_Length_2049	96.29	2050	9693	7644	100.0	0.0	3351.0